

Normal-Mode Vibrational Analysis of Weakly Bound Oligomers at Constrained Stationary Points of Arbitrary Order

Roland Tóbiás, Péter Árendás, and Attila G. Császár*



Cite This: *J. Chem. Theory Comput.* 2022, 18, 1788–1798



Read Online

ACCESS |



Metrics & More

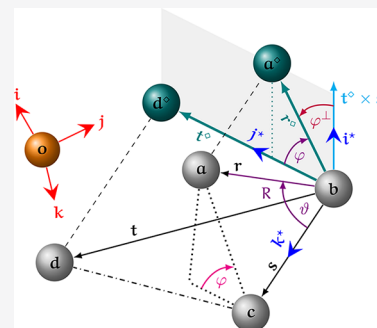


Article Recommendations



Supporting Information

ABSTRACT: Following the full realization of the importance of noncovalent interactions, finding and characterizing stationary points (SP), of various order, for weakly bound oligomers have become important tasks for computational chemists. An efficient algorithm and an associated computer code, called *oligoCGO*, are described, facilitating constrained geometry optimization of oligomers of arbitrary structure and complexity and normal-mode vibrational analysis at nonstationary geometries. To minimize the adverse effects of nonzero forces on harmonic vibrational analyses at constrained stationary points (cSP), two residual gradient correction (RGC) schemes are proposed. RGC₁, for which a rigorous justification is given, is based on ignoring the remaining forces in internal-coordinate space. RGC₂ modifies the geometry of the cSP in a single Newton step and recalculates the Cartesian Hessian at this updated geometry. As demonstrated by 10 examples related to the water–water, water–methane, and methane–methane dimers as well as the methane trimer, without RGC the harmonic analysis of cSPs may result in even qualitatively incorrect results when compared to reference values obtained at the nearby unconstrained SPs (uSP). Both RGC protocols work exceedingly well, and the corrected harmonic wavenumbers of the cSPs are very close to their uSP counterparts.



1. INTRODUCTION

One of the most powerful applications of quantum chemistry in molecular sciences concerns the determination of potential energy surfaces (PESs) and the exploration of the related nuclear dynamics.^{1–8} PESs, arising within the Born–Oppenheimer approximation,^{9,10} are functions representing the total energy of the system with respect to some or all nuclear degrees of freedom. High-quality PESs have been generated not only for molecules connected by covalent bonds¹¹ but also for (weakly bound) oligomers, assemblies of molecules held together by secondary chemical forces, whereby it is reasonable to assume that the monomers retain most of their individual structural and dynamical characteristics.

After the generation of PESs, it is usual to search for minima on them and characterize these stationary points (SPs) by computing the corresponding vibrational normal modes via the standard GF formalism.^{12,13} Nevertheless, PESs may have many more higher-order SPs than minima, most often there are only one or a few minima on a given PES, and these SPs are often responsible for interesting and important dynamical behavior.

It is customary to look for SPs, usually minima and first-order saddle points, via electronic-structure techniques without the desire to generate a complete surface. In fact, this is what most researchers do on a regular basis when utilizing the vast number of standard electronic-structure codes developed to produce reaction profiles. Determination and characterization of SPs of various order has a vast literature; see, for example,

refs 14–21. Nevertheless, it appears that there are still not fully explored issues related to the geometry optimization and characterization of constrained (reduced-dimensional) molecular models, as seen below.

A variety of so-called noncovalent interactions (NCIs),²² hydrogen bonds,²³ dihydrogen (H:H) bonds,^{24–26} CH \cdots π ,²⁷ $\pi\cdots\pi$ stacking,²⁸ halogen bonding,^{29,30} chalcogen bonding,³¹ salt bridges (ion pairing),³² agostic and anagostic interactions,³³ as well as perpendicular/coplanar cation– π (CP $_{\perp}$ /CP $_{\parallel}$) and anion– π (AP $_{\perp}$ /AP $_{\parallel}$) interactions,^{34–36} play a crucial role in many fields of chemistry. Intermolecular NCIs³⁷ are indispensable to understand materials science and important biochemical phenomena, such as protein folding, molecular recognition, and amyloid formation.

In order to minimize the computational effort, PESs of oligomers, held together by NCIs, are most often determined within the chemically intuitive rigid-monomer approximation (RMA, see ref 7 and references therein). Within the RMA, the dynamics of a dimer is at most a six-dimensional (6D) one, irrespective of the size of the monomers. These RMA-based model PESs give rise to constrained SPs (cSPs), which differ

Received: November 12, 2021

Published: February 24, 2022



only slightly from their “nearby” unconstrained SP (uSP) counterparts on the corresponding full-dimensional PES.

There are several reports^{21,38–45} about algorithms and codes capable of performing geometry optimizations with chemically guided structural constraints. Constrained geometry optimization is often employed in various areas of chemistry: computation of deformation energies, preliminary exploration of reaction paths and SPs, finding crossing points between two PESs, assessing ring-puckering distortions, etc. Nevertheless, to the best of our knowledge, issues related to nonzero forces associated with the harmonic vibrational analysis at cSPs have not been considered by the developers of constrained optimization techniques.

Due to the presence of unoptimized nuclear degrees of freedom (DOF), there are remaining forces at cSPs along some of the nuclear DOFs. This becomes an issue when a harmonic (normal-mode) vibrational analysis is performed at a cSP, as the standard GF method^{12,13} assumes that there are no forces present at the reference geometry.

In general, the nonzero-force dilemma⁴⁶ appears when force constants, that is, the derivatives of the total energy with respect to geometric variables,⁴⁷ are evaluated at nonstationary reference geometries, leading to ambiguities during the determination of harmonic¹³ as well as anharmonic^{47,48} vibrational wavenumbers. Nonetheless, as demonstrated in previous studies,^{1,46,49–51} and here once again, if the Cartesian Hessian is corrected with the nonzero gradient via appropriate procedures, the adverse effects of nonzero forces can be minimized.

One of the principal results of this study is the code `oligoCGO`, applicable for finding and characterizing cSPs of oligomers. The methodology utilized in `oligoCGO` is briefly outlined in section 2, while the technical details are provided in the extensive Supporting Information (SI). In section 2.4, two residual gradient correction (RGC) protocols are proposed for the effective computation of meaningful normal modes at cSPs. The RGC₁ method, which is based on the elimination of remaining forces in internal-coordinate space, is supported with a rigorous derivation in the Appendix. RGC₂ improves the cSP geometry in a single Newton step and re-evaluates the Cartesian Hessian at this modified geometry. The performance of the `oligoCGO` code is tested on 10 examples: the global minimum of the water dimer, two SPs of the water–methane dimer, five SPs of the methane dimer, and two SPs of the methane trimer. The numerical results, discussed in section 5, clearly demonstrate the utility of the `oligoCGO` code to find cSPs and to obtain physically correct normal modes in the presence of remaining forces.

2. METHODOLOGICAL CONSIDERATIONS

2.1. Representation of Oligomer Geometries. To describe the structural characteristics of oligomers, various coordinate specifications can be adopted. A possible choice is to define redundant internal coordinates,^{17,18,52,53} which are based on the bonding information on the monomers and the use of intermolecular coordinates. Another feasible representation relies on the separation of the inter- and intramolecular variables. This formalism considers the intermolecular motions similar to translations and rotations,⁵⁴ and applies carefully selected internal coordinates for the intramolecular motions.

In the approach chosen, the monomer geometries are described via internal coordinates. For each monomer, three virtual sites are specified, and the intramonomer coordinates

are related to them. In this case, a monomer structure can be rotated/translated by modifying the positions of its virtual sites. As a result, the internal coordinates describing the virtual-site positions represent the intermolecular degrees of freedom of the oligomer. The technical details of this approach are presented in sections S1–S4 of the SI. Our approach provides a general scheme to treat oligomers of arbitrary monomers (atomic, linear, and nonlinear), and it helps to avoid singularities due to 0/180° half (“bond”) angles via a careful and dynamically adjusted choice of internal coordinates.

2.2. Derivative Relations. Let the (rectilinear) Cartesian and the (curvilinear) internal coordinates of an oligomer be collected into the vectors $\mathbf{X} = \{X_1, X_2, \dots, X_C\}^T$ and $\mathbf{q} = \{q_1, q_2, \dots, q_Y\}^T$, respectively, where C and Y designate the number of Cartesian and internal coordinates, respectively. The internal coordinates are assumed to form a complete, but not necessarily nonredundant, set, describing all kinds of feasible motions of the oligomer.

It is well known^{1,46,55} that partial derivatives of the total energy E , with respect to nuclear DOFs, have the following relations:

$$\mathbf{g}_{\text{int}} = \mathbf{B}\mathbf{g}_{\text{Cart}} \quad (1)$$

$$\mathbf{H}_{\text{int}} = \mathbf{B}\mathbf{H}_{\text{Cart}}\mathbf{B}^T + \mathbf{B}^{(2)}\mathbf{g}_{\text{Cart}} \quad (2)$$

where $\mathbf{B} = \{\partial X_i/\partial q_k\}$ denotes the El'yashevich–Wilson B matrix,^{12,13} $\mathbf{g}_{\text{int}} = \{\partial E/\partial q_k\}$ and $\mathbf{g}_{\text{Cart}} = \{\partial E/\partial X_i\}$ are internal and Cartesian gradients, respectively, $\mathbf{B}^{(2)} = \{\partial^2 X_i/\partial q_k \partial q_l\}$, while $\mathbf{H}_{\text{int}} = \{\partial^2 E/\partial q_k \partial q_l\}$ and $\mathbf{H}_{\text{Cart}} = \{\partial^2 E/\partial X_i \partial X_j\}$ indicate the internal and Cartesian Hessians, respectively. By employing the tensors $\mathbf{A} = \{\partial q_k/\partial X_i\}$ and $\mathbf{A}^{(2)} = \{\partial^2 q_k/\partial X_i \partial X_j\}$, eqs 1 and 2 can be inverted,^{1,55}

$$\mathbf{g}_{\text{Cart}} = \mathbf{A}\mathbf{g}_{\text{int}} \quad (3)$$

$$\mathbf{H}_{\text{Cart}} = \mathbf{A}\mathbf{H}_{\text{int}}\mathbf{A}^T + \mathbf{A}^{(2)}\mathbf{g}_{\text{int}} \quad (4)$$

Combining eq 1 and 3 into $\mathbf{g}_{\text{Cart}} = \mathbf{A}\mathbf{g}_{\text{int}} = \mathbf{A}\mathbf{B}\mathbf{g}_{\text{Cart}}$ suggests that $\mathbf{A}\mathbf{B} = \mathbf{I}^{C \times C}$ for a general \mathbf{g}_{Cart} where $\mathbf{I}^{C \times C}$ is the $C \times C$ identity matrix. To show that $\mathbf{A}^{(2)}$ is dependent on $\mathbf{B}^{(2)}$, let us substitute eqs 1 and 2 into eq 4 leading to,

$$\begin{aligned} \mathbf{H}_{\text{Cart}} &= \mathbf{A}\mathbf{B}\mathbf{H}_{\text{Cart}}\mathbf{B}^T\mathbf{A}^T + \mathbf{A}\mathbf{B}^{(2)}\mathbf{g}_{\text{Cart}}\mathbf{A}^T + \mathbf{A}^{(2)}\mathbf{B}\mathbf{g}_{\text{Cart}} \\ &= \mathbf{H}_{\text{Cart}} + [\mathbf{C} + \mathbf{A}^{(2)}\mathbf{B}]\mathbf{g}_{\text{Cart}} \end{aligned} \quad (5)$$

where the \mathbf{C} tensor is defined to satisfy $\mathbf{A}\mathbf{B}^{(2)}\mathbf{g}_{\text{Cart}}\mathbf{A}^T = \mathbf{C}\mathbf{g}_{\text{Cart}}$. As \mathbf{g}_{Cart} is arbitrary, eq 5 implies $\mathbf{C} = -\mathbf{A}^{(2)}\mathbf{B}$. For further details about derivative relations, see section S5 and, for higher orders in particular, ref 55.

2.3. Finding Constrained Stationary Points of Oligomers. A number of sophisticated procedures have been suggested^{14,18,21,38,40,41,44,56,57} to facilitate the determination of constrained and unconstrained SPs on multivariable PESs. The majority of these algorithms are built upon the use of quasi-Newton methods and redundant internal coordinates. However, the geometry optimization of weakly bound oligomers may need second-order partial derivatives (or beyond) to ensure better convergence.

In the present study, the oligomer geometries are optimized, with respect to an internal-coordinate subspace, via the traditional Newton–Raphson (NR) scheme, which does not need a guess for the order of the yet-to-be-identified cSP.

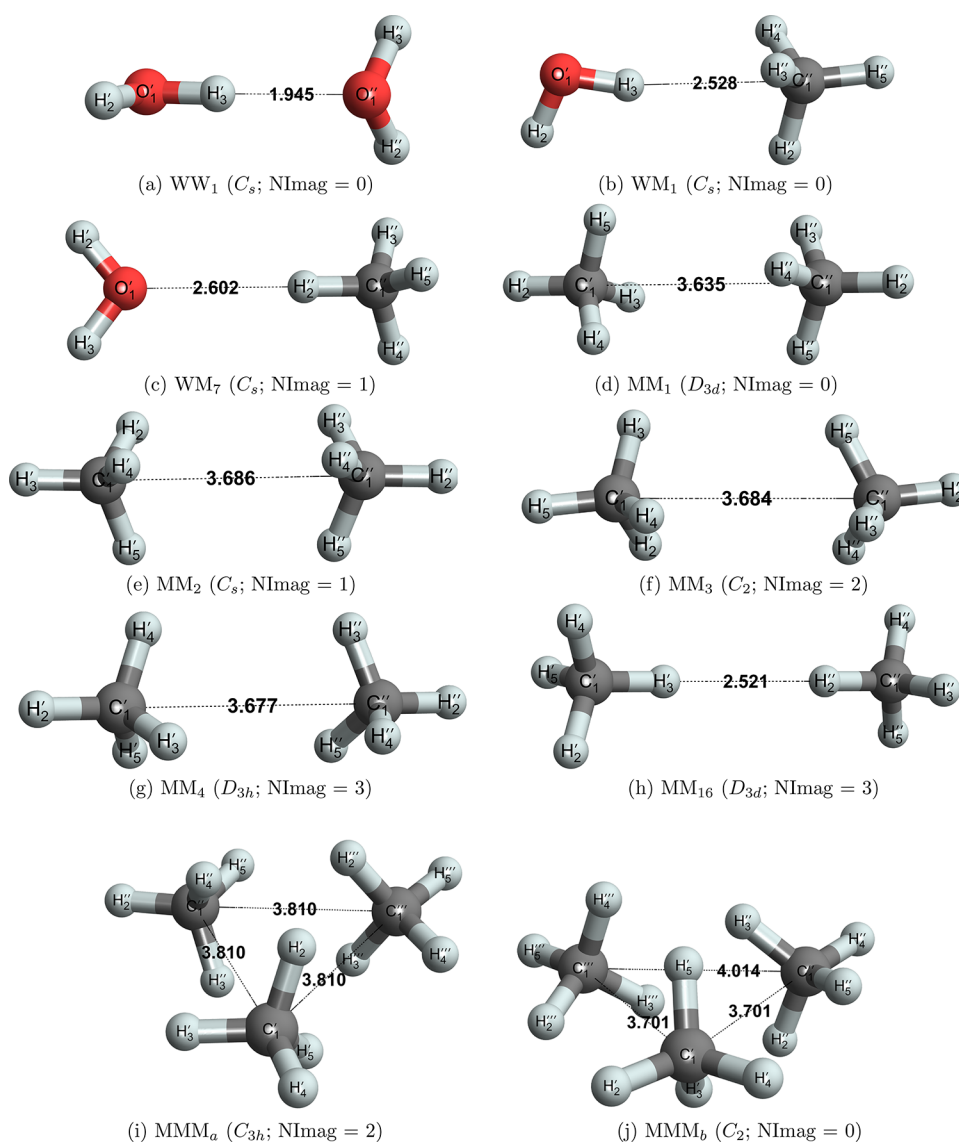


Figure 1. Stationary points of oligomers examined in the present study. WW = water dimer, WM = water–methane dimer, MM = methane dimer, MMM = methane trimer. The point groups and the number of imaginary modes (NImag) are given in parentheses. The distances between certain atoms connected by a dotted line are given in Å.

While the NR method provided fast convergence in our test cases, the use of Hessian update formulas (e.g., that in eqs 19 and 20 of ref 58) cannot be avoided for larger oligomers. For further details on finding cSPs, see section S6 of the SI.

2.4. Normal-Mode Analysis at Constrained Stationary Points. Geometry optimizations are often followed by a normal-mode vibrational analysis of the SP. These computations help (a) the characterization of the SPs identified through the analysis of the Hessian eigenvalues (usually called “second-derivative tests”) and (b) the qualitative understanding of the internal motions around the SPs. Normal coordinates also form the basis of deriving higher-order (ro)vibrational corrections.⁴⁸

Standard harmonic vibrational analysis^{12,13} is designed for uSPs, where \mathbf{g}_{Cart} or, equivalently, \mathbf{g}_{int} is a zero vector. At a cSP, the norm of \mathbf{g}_{Cart} is small but not zero, which must be accounted for. Based on refs 46 and 59, possible ways to treat the residual gradient of cSPs are outlined. The schemes proposed are variants of what we call residual gradient corrections (RGC). The principal role of RGCs is to make

the normal modes of a cSP as close to their unconstrained (uSP) counterparts as feasible.

Suppose that there is a uSP close to the cSP examined and denote the Cartesian coordinate vectors of this (cSP, uSP) pair with $(\mathbf{X}, \mathbf{X}^*)$. Similarly, let the Cartesian gradient and Hessian matrix at \mathbf{X}^* be distinguished from those at \mathbf{X} with an asterisk. Clearly, $\mathbf{g}_{\text{Cart}}^* = \mathbf{0}$, while $\mathbf{H}_{\text{Cart}}^*$ can be estimated with what we call the RGC₀ scheme:

$$\mathbf{H}_{\text{Cart}}^* \approx \mathbf{H}_{\text{Cart}} + \mathbf{T}_{\text{Cart}}(\mathbf{X}^* - \mathbf{X}) \approx \mathbf{H}_{\text{Cart}} - \mathbf{T}_{\text{Cart}}\mathbf{H}_{\text{Cart}}^{-1}\mathbf{g}_{\text{Cart}} \quad (6)$$

where \mathbf{T}_{Cart} is the tensor including the third-order Cartesian partial derivatives of E at \mathbf{X} , and $\mathbf{X}^* - \mathbf{X}$ is approximated with the Newton correction, $-\mathbf{H}_{\text{Cart}}^{-1}\mathbf{g}_{\text{Cart}}$. From the estimated $\mathbf{H}_{\text{Cart}}^*$ matrix, the normal-mode vibrational wavenumbers of the cSP studied can be derived, as detailed, for example, in ref 60. Note that, during the construction of the inertia tensor and the projection matrix, one can apply the entries of \mathbf{X} , estimating the components of the unknown vector \mathbf{X}^* .

Table 1. Comparison of Selected Quantum-Chemical Quantities Characterizing the Global Minimum, WW₁, of the Water Dimer, Obtained via Different Approaches^{ab}

quantity	noRGC(c)	RGC ₁	RGC ₂	noRGC(u)
ΔE_{inter}	-1798.942	see noRGC(c)	-1811.998	-1812.011
GRMSD	5.81	see noRGC(c)	1.10	0.00
mode #1 (<i>a''</i>)	152.285 [0.765]	126.741 [1.000]	127.524 [0.998]	126.980
mode #2 (<i>a''</i>)	-135.844 [0.761]	145.345 [1.000]	147.165 [0.998]	147.081
mode #3 (<i>a'</i>)	92.585 [0.866]	153.295 [1.000]	154.849 [1.000]	154.915
mode #4 (<i>a'</i>)	173.529 [0.876]	181.455 [1.000]	184.110 [1.000]	184.164
mode #5 (<i>a'</i>)	317.598 [0.982]	355.534 [1.000]	359.962 [1.000]	360.379
mode #6 (<i>a''</i>)	549.487 [0.995]	625.170 [1.000]	628.621 [1.000]	630.336
mode #7 (<i>a'</i>)	1630.392 [0.996]	1636.701 [0.999]	1629.392 [1.000]	1629.307
mode #8 (<i>a'</i>)	1645.860 [0.996]	1661.585 [0.999]	1650.025 [1.000]	1650.269
mode #9 (<i>a'</i>)	3796.397 [0.956]	3796.385 [0.956]	3720.772 [1.000]	3718.730
mode #10 (<i>a'</i>)	3828.381 [0.988]	3828.355 [0.988]	3813.693 [1.000]	3813.925
mode #11 (<i>a'</i>)	3921.950 [0.963]	3921.813 [0.963]	3915.037 [1.000]	3915.150
mode #12 (<i>a''</i>)	3945.934 [1.000]	3945.786 [1.000]	3935.000 [1.000]	3935.281

^anoRGC(c) = Hessian computed at the constrained optimum without residual gradient correction (RGC); RGC₁ = RGC₁-corrected Hessian; RGC₂ = RGC₂-corrected geometry and Hessian; noRGC(u) = Hessian at the unconstrained optimum without RGC. The interaction energies, ΔE_{inter} , in cm⁻¹, correspond to the geometries of the different schemes. GRMSDs, in mÅ, are the geometric root-mean square deviations⁶⁷ of the various oligomer structures with respect to the unconstrained optimum, calculated at optimal alignments and atomic orderings, called here "best orientations". ^bThe last 12 rows contain normal-mode vibrational wavenumbers, in cm⁻¹, computed with the four schemes and ordered according to the increasing absolute values of the last column. Negative wavenumbers are imaginary values. The vibrational symmetry labels are displayed in the first column in parentheses. Utilizing the best orientations, the normal modes derived via the noRGC(c), RGC₁, and RGC₂ protocols were matched with their noRGC(u) counterparts, based on the overlaps between the normal-mode eigenvectors. These overlaps are indicated in square brackets in columns 2–4.

As shown in the Appendix, the following approximation can be employed to \mathbf{T}_{Cart} :

$$\mathbf{T}_{\text{Cart}} \approx \mathbf{A}^{(2)} \mathbf{B} \mathbf{H}_{\text{Cart}} \quad (7)$$

This approximation results in what we call the RGC₁ scheme:

$$\mathbf{H}_{\text{Cart}}^* \approx \mathbf{H}_{\text{Cart}} - \mathbf{A}^{(2)} \mathbf{B} \mathbf{g}_{\text{Cart}} = \mathbf{H}_{\text{Cart}} - \mathbf{A}^{(2)} \mathbf{g}_{\text{int}} = \mathbf{A} \mathbf{H}_{\text{int}} \mathbf{A}^T \quad (8)$$

In fact, RGC₁ reflects the recommendation^{1,46} that to handle the nonzero-force dilemma the second term of eq 4 must be omitted. The numerical results of ref 46 and this study, *vide infra*, demonstrate that RGC₁ indeed provides a good estimate of $\mathbf{H}_{\text{Cart}}^*$ when the internal coordinates are chosen reasonably.

Another scheme, called RGC₂, can also be specified. RGC₂ is based on the construction of the Cartesian Hessian, $\mathbf{H}_{\text{Cart}}^{\circ}$, at the point $\mathbf{X}^{\circ} = \mathbf{X} - \mathbf{H}_{\text{Cart}}^{-1} \mathbf{g}_{\text{Cart}}$. This \mathbf{X}° point mimics \mathbf{X}^* well if \mathbf{X} lies in the quadratic region of \mathbf{X}^* on the PES. While RGC₂ is more expensive than RGC₁, due to the need to compute the Hessian twice, RGC₂ has the advantage that it can be easily implemented in standard electronic-structure codes. In the rest of this paper, the RGC₁ and RGC₂ schemes are utilized to correct \mathbf{H}_{Cart} and approximate $\mathbf{H}_{\text{Cart}}^*$.

3. THE OLIGOCGO CODE

Based on the background information outlined in section 2 and in more detail in sections S1–S6 of the SI, a special-purpose code called `oligoCGO`, standing for Constrained Geometry Optimization for oligomers, has been developed. Some special features of `oligoCGO` are as follows: (a) it can redefine the half angles when they approach 0/180° during the optimizations (see Secs. S4 and S6 of the SI), (b) it determines the order of the cSP by analyzing the eigenvalues of the reduced-dimensional internal Hessian, and (c) it corrects the vibrational fundamentals via the RGC₁ and RGC₂ protocols. At present, the `oligoCGO` code supports only local optimizations. Nevertheless, we plan to implement a global optimization scheme, like the one in ref 54, for PESs which can be evaluated at a reasonable cost.

During this study, the electronic-structure computations required by `oligoCGO` have been accomplished with the Gaussian16 code⁶¹ but `oligoCGO` could also be employed with any other packages. The Cartesian gradients and Hessians are determined analytically and extracted automatically from the formatted checkpoint file. During the optimization steps, the option 'sym=None' is used, ensuring that the input orientation is preserved.

Upon termination of the constrained geometry optimization, the point-group symmetry of the cSP is identified with the

Table 2. Comparison of Selected Quantum-Chemical Quantities, Obtained for the Global Minimum of the Water Dimer, WW₁, by Relaxing the Interacting (donor) O₁–H₂ Stretch Coordinate^a

quantity	noRGC(c)	RGC ₁	RGC ₂	noRGC(u)
ΔE_{inter}	−1809.770	see noRGC(c)	−1812.010	−1812.011
GRMSD	2.97	see noRGC(c)	0.41	0.00
mode #1 (a'')	147.686 [0.709]	127.516 [0.999]	127.444 [1.000]	126.980
mode #2 (a'')	22.635 [0.709]	146.821 [0.999]	147.737 [1.000]	147.081
mode #3 (a')	152.414 [0.997]	154.535 [1.000]	155.435 [1.000]	154.915
mode #4 (a')	181.860 [0.997]	183.616 [1.000]	184.520 [1.000]	184.164
mode #5 (a')	365.029 [0.999]	359.462 [1.000]	360.825 [1.000]	360.379
mode #6 (a'')	627.917 [1.000]	628.887 [1.000]	630.629 [1.000]	630.336
mode #7 (a')	1630.891 [1.000]	1636.284 [0.998]	1629.379 [1.000]	1629.307
mode #8 (a')	1654.553 [1.000]	1653.650 [0.998]	1650.272 [1.000]	1650.269
mode #9 (a')	3717.256 [1.000]	3717.229 [1.000]	3718.380 [1.000]	3718.730
mode #10 (a')	3827.402 [1.000]	3827.377 [1.000]	3813.668 [1.000]	3813.925
mode #11 (a')	3903.134 [1.000]	3903.037 [1.000]	3915.136 [1.000]	3915.150
mode #12 (a'')	3945.897 [1.000]	3945.744 [1.000]	3935.001 [1.000]	3935.281

^aThe definition of the atoms O₁ and H₂ is shown in Figure 1a. For all the other abbreviations, see footnote a to Table 1.

SYVA (SYmmetry analyzer using Vector Algebra⁶³)⁶² code in an automated way (the distortion tolerance parameter^{62,63} is set to 2 mÅ). After recognition of the highest point group, the analyzed geometry is symmetrized by SYVA and replaces that obtained by `oligoCGO`. Following the computation of the Cartesian gradients and Hessians at a cSP, the SYVA-based geometry is transformed into the standard orientation utilized by Gaussian16. At cSPs, both uncorrected and RGC-corrected normal modes are computed by the `oligoCGO` code.

4. COMPUTATIONAL DETAILS

As test cases, the numerical part of the present study employs the oligomers WW, WM, MM, and MMM (see Figure 1). The initial structures of the SPs investigated were taken from the rigid-monomer PESs reported in ref 64 for WW, WM, and MM or constructed manually in the case of MMM. The intramolecular internal coordinates of the monomers were set to the equilibrium values related to the frozen-core Møller–Plesset (MP2)⁶⁵ level, utilizing the aug-cc-pVTZ⁶⁶ basis set. The aug-cc-pVTZ MP2 optimizations have been performed for the isolated monomers with the Gaussian16 code.⁶¹

All of the constrained geometry optimizations and RGC analyses of this study utilized the code `oligoCGO`. The total energies necessary for geometry optimizations and harmonic vibrational analyses have been obtained at the aug-cc-pVTZ MP2 level, without consideration of the basis-set-superposition error.^{68,69}

The oligomer structures examined were also subject to unconstrained optimization through separate execution of Gaussian16,⁶¹ applying the directive ‘opt = VeryTight’. The uSPs identified were then read in by `oligoCGO` to determine their Cartesian Hessians and calculate the normal modes. These wavenumbers serve as reference values to be compared with their RGC₁ and RGC₂ siblings. At the end of the `oligoCGO` output file, a table is given reporting the vibrational fundamentals yielded by the different methods. These output files, together with a description of the file contents in Sec. S7, form part of the SI.

5. RESULTS AND DISCUSSION

For the 10 structures shown in Figure 1, the most important quantum-chemical quantities of the present study, that is, the interaction energies (ΔE_{inter}), the geometric root-mean square

deviations (GRMSDs), and the normal-mode vibrational fundamentals, are calculated at the respective cSPs and uSPs as well as at the RGC₂-corrected geometries. In what follows, the computational results obtained for cSPs and uSPs are referenced with tags “noRGC(c)” and “noRGC(u)”, respectively, while the data computed with the RGC₁ and RGC₂ schemes are labeled “RGC₁” and “RGC₂”, respectively. The noRGC(c), RGC₁, and RGC₂ normal modes are matched with their noRGC(u) counterparts by finding the maximum overlaps (unsigned dot products) between the associated normal-mode eigenvectors.

5.1. Water Dimer, WW. Of the 13 SPs identified on the WW19 PES of ref 64, only the lowest-energy SP, designated here as WW₁ (see Figure 1a), is investigated. WW₁ is the only minimum on the PES and it is characterized by a relatively strong H-bond with large intermolecular wavenumbers (see Table 1).

Alarming, if the residual Cartesian gradient is not considered at the cSP of WW₁, optimized within the rigid-monomer approximation, a spurious imaginary fundamental, around 136 i cm^{−1} (mode #2), is obtained, with a poor overlap of just 0.76 between the appropriate noRGC(c) and noRGC(u) normal-mode eigenvectors.

When RGC₁ is employed, the imaginary wavenumber of mode #2 becomes real and the intermolecular fundamentals computed are all very close to their counterparts determined at the uSP, with fairly high overlaps between the eigenvectors. It is an important observation that the RGC₁ protocol does not improve the intramolecular modes, or even contaminates some of them with an extra error of 1–7 cm^{−1}.

The fourth column of Table 1 clearly shows that RGC₂ (see the last paragraph of section 2.4) almost completely remedies the inaccuracy of the intramolecular modes while further reducing the error in the intermolecular fundamentals. The improvements appear to be connected to the GRMSDs, as the RGC₂ method is characterized by a GRMSD value that is an order of magnitude smaller than that of noRGC(c). Obviously, the RGC₂ method must work well if the cSP is in the quadratic regime of the PES. This is seemingly the case for WW₁, where RGC₂ brings the interaction energy as close as 0.01 cm^{−1} to the noRGC(u) reference value.

An alternative route to decrease the discrepancy observed for mode #9 (i.e., the O₁–H₂ stretch fundamental; see Figure

Table 3. Six Intermolecular Fundamentals Pertaining to the Unique Minimum of the Water Dimer, WW_1 , Obtained via the RGC_1 Scheme with Alternative Internal-Coordinate Systems^a

quantity	RGC_1	$RGC_1(\text{alt-1})$	$RGC_1(\text{alt-2})$	$RGC_1(\text{alt-3})$	noRGC(u)
mode #1 (a'')	126.741 [1.000]	126.696 [1.000]	126.741 [1.000]	126.740 [1.000]	126.980
mode #2 (a'')	145.345 [1.000]	145.768 [0.999]	145.346 [1.000]	145.346 [1.000]	147.081
mode #3 (a')	153.295 [1.000]	155.169 [0.992]	164.843 [0.789]	153.298 [1.000]	154.915
mode #4 (a')	181.455 [1.000]	188.975 [0.993]	297.764 [0.779]	181.445 [1.000]	184.164
mode #5 (a')	355.534 [1.000]	355.964 [1.000]	357.811 [0.987]	355.530 [1.000]	360.379
mode #6 (a'')	625.170 [1.000]	625.215 [1.000]	625.170 [1.000]	625.170 [1.000]	630.336

^aThe wavenumbers of columns “ RGC_1 ” and “noRGC(u)” are copied from Table 1. Columns “ $RGC_1(\text{alt-1})$ ”, “ $RGC_1(\text{alt-2})$ ”, and “ $RGC_1(\text{alt-3})$ ” comprise the results obtained with three alternative internal-coordinate systems, whose definitions are included in the appropriate `oligoCGO` output files. The boldface entries have relatively large errors, when compared to the noRGC(u) reference values (see the last column of the table).

Table 4. Comparison of Selected Quantum-Chemical Quantities Determined for the First (WM_1) and Seventh (WM_7) Lowest-Energy Stationary Points of the Water–Methane Dimer^a

species	quantity	noRGC(c)	RGC_1	RGC_2	noRGC(u)
WM_1 (C_s) [see Figure 1b]	ΔE_{inter}	−400.610	see noRGC(c)	−405.301	−405.301
	GRMSD	4.01	see noRGC(c)	0.55	0.00
	mode #1 (a'')	−35.889 [0.999]	22.759 [1.000]	24.297 [1.000]	23.593
	mode #2 (a')	73.653 [0.977]	79.898 [0.989]	80.297 [0.999]	80.038
	mode #3 (a')	67.891 [0.934]	85.646 [0.989]	86.492 [0.999]	86.087
	mode #4 (a'')	72.500 [0.975]	94.038 [1.000]	95.087 [1.000]	94.786
	mode #5 (a')	104.230 [0.925]	117.976 [1.000]	119.855 [1.000]	119.827
	mode #6 (a'')	148.944 [0.975]	172.954 [1.000]	176.735 [1.000]	176.538
WM_7 (C_s) [see Figure 1c]	ΔE_{inter}	−258.949	see noRGC(c)	−260.045	−260.038
	GRMSD	47.59	see noRGC(c)	47.57	0.00
	mode #1 (a'')	−58.861 [0.987]	6.916 [0.839]	7.225 [0.862]	−3.629
	mode #2 (a')	−45.569 [0.988]	−12.050 [0.847]	−12.125 [0.866]	9.012
	mode #3 (a'')	−61.607 [0.994]	13.057 [0.893]	13.553 [0.914]	11.326
	mode #4 (a')	72.267 [1.000]	72.301 [0.999]	72.569 [0.999]	72.500
	mode #5 (a')	57.476 [0.994]	91.941 [0.996]	92.469 [0.996]	92.087
	mode #6 (a'')	97.144 [0.995]	118.185 [0.996]	119.014 [0.996]	118.388

^aSee footnote *a* to Table 1 for the abbreviations and the definitions of the quantities.

1a) is to optimize the O_1-H_2 distance. As observed in Table 2, this modification improves significantly the noRGC(c) and RGC_1 estimates for mode #9.

To analyze the effects the choice of different internal-coordinate systems has on the RGC_1 fundamentals, three alternative *Z* matrices have been constructed by modifying the “default” specification introduced in section S4. The intermolecular modes related to the default and the alternative internal-coordinate systems are shown in Table 3. The definitions of the modified coordinates are given in the `oligoCGO` output files. To enhance readability, significant errors are typeset in bold. Although the origin of the differences is not obvious, it is reassuring that utilizing “chemically meaningful” internal coordinates in the RGC_1 scheme provides excellent estimates of the fundamentals.

The fact that accurate results are obtained for the interaction energy and the vibrational fundamentals of WW_1 via the RGC schemes is encouraging. While there are oligomers with considerably stronger H bonds, WW can be viewed as an unfavorable case in the world of constrained optimizations. In other words, the discrepancies from the fully geometry optimized results are expected to be smaller for systems containing much more rigid monomers.

5.2. Water–Methane Dimer, WM . From the 25 SPs identified on the WM_{19} PES,⁶⁴ the first and the seventh lowest-energy SP, WM_1 , and WM_7 , respectively, are studied

here. WM_1 , whereby the water molecule plays the role of the H-bond donor, is definitely the global minimum on the real PES of WM . The order of the WM_7 SP, whereby the H-bond donor is the methane molecule, is less clear.

While several studies^{70–73} consider WM_7 as a secondary minimum of WM , the Hessian on the WM_{19} PES corresponding to WM_7 is characterized by a small negative eigenvalue. An unconstrained aug-cc-pVTZ MP2 geometry optimization and the subsequent harmonic vibrational analysis yields one imaginary fundamental, 3.6 i cm^{-1} , for WM_7 , in line with the WM_{19} PES. At the aug-cc-pVQZ MP2 level, employing a significantly larger basis, the same fundamental, related to the (almost free) rotation of the water monomer around the $C_1''-H_1''$ axis, becomes real, is 2.9 cm^{-1} . To ascertain the true order of WM_7 further electronic-structure computations, much closer to the complete-basis-set full-configuration-interaction limit, would be required. This task is beyond the scope of the present study.

As is clear from Table 4, the interaction energies of WM_1 and WM_7 are significantly smaller, by more than a factor of 4, than that of WW_1 . The intermolecular fundamentals of WM_1 exhibit a similar behavior, at least in a qualitative sense, to those determined for WW_1 : (a) when the residual gradient is ignored in Cartesian space, the underlying cSP is characterized by an imaginary mode (mode #1), although the uSP structure is a minimum; (b) the RGC_1 scheme produces highly accurate

Table 5. Comparison of Selected Quantum-Chemical Quantities Determined for Five Stationary Points of the Methane Dimer (MM) via Different Approaches^a

species	quantity	noRGC(c)	RGC ₁	RGC ₂	noRGC(u)
MM ₁ (<i>D</i> _{3d}) [see Figure 1d]	ΔE_{inter}	-210.225	see noRGC(c)	-210.581	-210.581
	GRMSD	1.22	see noRGC(c)	0.00	0.00
	mode #1 (<i>e_g</i>)	19.027 [0.962]	43.401 [0.965]	43.639 [0.950]	43.612
	mode #2 (<i>e_g</i>)	19.028 [0.962]	43.401 [0.965]	43.636 [0.950]	43.612
	mode #3 (<i>a_{1u}</i>)	46.241 [1.000]	44.482 [1.000]	44.686 [1.000]	44.661
	mode #4 (<i>a_{1g}</i>)	65.774 [1.000]	65.774 [1.000]	65.907 [1.000]	65.906
	mode #5 (<i>e_u</i>)	56.368 [0.860]	69.269 [0.974]	69.518 [0.982]	69.502
MM ₂ (<i>C_s</i>) [see Figure 1e]	ΔE_{inter}	-196.077	see noRGC(c)	-196.380	-196.380
	GRMSD	2.17	see noRGC(c)	0.96	0.00
	mode #1 (<i>a'</i>)	-36.966 [0.798]	9.376 [1.000]	11.594 [1.000]	10.181
	mode #2 (<i>a''</i>)	-26.108 [0.996]	25.085 [1.000]	26.603 [1.000]	26.498
	mode #3 (<i>a''</i>)	-18.501 [0.799]	-28.972 [1.000]	-28.933 [1.000]	-29.324
	mode #4 (<i>a'</i>)	65.664 [0.763]	64.887 [1.000]	65.072 [1.000]	65.045
	mode #5 (<i>a'</i>)	62.611 [0.761]	73.825 [1.000]	73.749 [1.000]	73.956
MM ₃ (<i>C₂</i>) [see Figure 1f]	ΔE_{inter}	-196.053	see noRGC(c)	-196.353	-196.353
	GRMSD	2.28	see noRGC(c)	0.82	0.00
	mode #1 (<i>b</i>)	-37.018 [0.999]	-10.875 [1.000]	-9.631 [1.000]	-11.689
	mode #2 (<i>a</i>)	-29.818 [0.724]	25.548 [1.000]	27.258 [1.000]	27.223
	mode #3 (<i>a</i>)	-16.013 [0.726]	-28.498 [1.000]	-28.251 [1.000]	-28.707
	mode #4 (<i>a</i>)	64.344 [0.983]	64.826 [1.000]	65.012 [1.000]	64.988
	mode #5 (<i>b</i>)	63.947 [0.999]	74.092 [1.000]	74.045 [1.000]	74.213
MM ₄ (<i>D</i> _{3h}) [see Figure 1g]	ΔE_{inter}	-195.749	see noRGC(c)	-196.018	-196.018
	GRMSD	1.01	see noRGC(c)	0.00	0.00
	mode #1 (<i>e''</i>)	-38.704 [0.924]	-17.525 [0.963]	-17.413 [0.994]	-17.470
	mode #2 (<i>e''</i>)	-38.702 [0.924]	-17.524 [0.963]	-17.400 [0.994]	-17.471
	mode #3 (<i>a''₁</i>)	-19.785 [1.000]	-28.364 [1.000]	-28.395 [1.000]	-28.508
	mode #4 (<i>a'₁</i>)	64.188 [1.000]	64.188 [1.000]	64.288 [1.000]	64.289
	mode #5 (<i>e'</i>)	72.075 [0.907]	80.367 [0.953]	80.554 [0.996]	80.538
MM ₁₆ (<i>D</i> _{3d}) [see Figure 1h]	ΔE_{inter}	-94.864	see noRGC(c)	-94.917	-94.917
	GRMSD	0.47	see noRGC(c)	0.00	0.00
	mode #1 (<i>a_{1u}</i>)	-23.279 [1.000]	-4.243 [1.000]	-5.290 [1.000]	-4.678
	mode #2 (<i>e_g</i>)	-15.624 [0.994]	-12.001 [0.998]	-11.509 [1.000]	-11.236
	mode #3 (<i>e_g</i>)	-15.627 [0.994]	-12.003 [0.998]	-11.512 [1.000]	-11.239
	mode #4 (<i>e_u</i>)	11.192 [0.993]	15.118 [0.996]	14.982 [1.000]	15.193
	mode #5 (<i>e_u</i>)	11.196 [0.993]	15.120 [0.996]	14.985 [1.000]	15.196
	mode #6 (<i>a_{1g}</i>)	44.957 [1.000]	44.957 [1.000]	44.977 [1.000]	45.004

^aSee footnote *a* to Table 1 for the abbreviations and the definitions of the quantities considered.

wavenumber estimates; and (c) the RGC₂ protocol provides a geometry which almost fully coincides with its uSP counterpart.

As a warning against the blind acceptance of the RGC₁ and RGC₂ estimates, for WM₇ the situation is considerably less favorable than found for WW₁ and WM₁. Though the deviation of the RGC₂ interaction energy from its noRGC(u) pair is minuscule, the RGC₁/RGC₂ wavenumbers exhibit significant errors, giving qualitatively incorrect results for modes #1–#3.

5.3. Methane Dimer, MM. For MM, results have been obtained for five selected SPs, namely, MM₁ (*D*_{3d}), MM₂ (*C_s*), MM₃ (*C₂*), MM₄ (*D*_{3h}), and MM₁₆ (*D*_{3d}), out of the 17 SPs found on the MM19 PES.⁶⁴ All these SPs have dihydrogen

(H:H) contacts,²⁶ ensuring limited stability, with $|\Delta E_{\text{inter}}| < 250 \text{ cm}^{-1}$.

The only minimum of the MM19 PES, MM₁, belongs to the *D*_{3d} point group. The three Hs of each monomer interact in a staggered configuration; this interaction scheme is denoted here as 3:3s. Despite the fairly small monomer deformations, the discrepancies of the noRGC(c) and noRGC(u) modes (see Table 5) are significant for the degenerate modes, more than 10 cm⁻¹. For MM₁, the deviations of the RGC₁ and RGC₂ fundamentals from the noRGC(u) results are never larger than 0.25 cm⁻¹.

The next three SPs, MM₂, MM₃, and MM₄, exhibit quite similar monomer orientations, with almost identical interaction energies, where three Hs of the monomers are “connected” in

Table 6. Comparison of Selected Quantum-Chemical Quantities Determined for Two Stationary Points of the Methane Trimer (MMM)^a

species	quantity	noRGC(c)	RGC ₁	RGC ₂	noRGC(u)
MMM _a (C _{3h}) [see Figure 1i]	ΔE_{inter}	-541.246	see noRGC(c)	-542.337	-542.337
	GRMSD	1.53	see noRGC(c)	0.02	0.00
	mode #1 (e'')	-35.530 [0.990]	-8.987 [0.999]	-6.095 [1.000]	-6.796
	mode #2 (e'')	-35.535 [0.990]	-9.003 [0.999]	-6.125 [1.000]	-6.817
	mode #3 (e')	-37.144 [0.693]	42.394 [0.805]	42.625 [0.900]	42.594
	mode #4 (e')	-37.149 [0.693]	42.391 [0.805]	42.623 [0.900]	42.595
	mode #5 (a'')	44.020 [0.995]	48.964 [1.000]	49.387 [1.000]	49.317
	mode #6 (e')	55.523 [0.720]	59.942 [0.724]	60.146 [0.908]	60.133
	mode #7 (e')	55.523 [0.720]	59.941 [0.724]	60.145 [0.908]	60.134
	mode #8 (e'')	58.547 [0.857]	62.040 [0.936]	62.342 [0.967]	62.278
	mode #9 (e'')	58.547 [0.857]	62.041 [0.936]	62.343 [0.967]	62.279
	mode #10 (a')	74.738 [0.708]	70.443 [1.000]	70.714 [1.000]	70.702
	mode #11 (a')	48.907 [0.708]	80.931 [1.000]	81.267 [1.000]	81.254
mode #12 (a'')	84.555 [0.995]	91.461 [1.000]	91.790 [1.000]	91.731	
MMM _b (C ₂) [see Figure 1j]	ΔE_{inter}	-540.595	see noRGC(c)	-541.514	-541.515
	GRMSD	1.57	see noRGC(c)	1.32	0.00
	mode #1 (b)	-2.858 [0.711]	20.909 [1.000]	21.706 [1.000]	21.149
	mode #2 (b)	-32.303 [0.721]	31.427 [1.000]	32.131 [1.000]	31.971
	mode #3 (b)	-42.496 [0.620]	35.843 [1.000]	36.332 [1.000]	36.105
	mode #4 (a)	34.588 [0.935]	36.896 [1.000]	37.024 [1.000]	36.987
	mode #5 (a)	10.877 [0.943]	41.268 [1.000]	41.864 [1.000]	41.659
	mode #6 (b)	26.736 [0.915]	55.056 [1.000]	55.440 [1.000]	55.240
	mode #7 (a)	40.399 [0.865]	60.431 [1.000]	60.700 [0.999]	60.583
	mode #8 (a)	61.263 [0.889]	63.558 [1.000]	64.112 [0.999]	63.795
	mode #9 (a)	70.471 [0.950]	72.101 [1.000]	72.412 [1.000]	72.318
	mode #10 (b)	70.628 [0.686]	80.615 [1.000]	81.053 [0.999]	80.892
	mode #11 (b)	73.636 [0.693]	83.519 [1.000]	83.886 [0.999]	83.785
mode #12 (a)	82.060 [0.963]	88.254 [1.000]	88.492 [1.000]	88.468	

^aSee footnote a to Table 1 for the abbreviations and the definitions of the quantities considered.

an eclipsed form. Therefore, these structures are called 3:3e. The main difference among the three SPs is in their point groups. As the point-group symmetry increases, the number of imaginary modes also increases, as expected. Surprisingly, the noRGC(c) estimates of modes #1–#3 are very similar for the three SPs, falsely ranking these structures as third-order SPs. Using the RGC schemes, accurate wavenumbers are obtained for these SPs, as well.

In the second-highest-energy SP of MM, MM₁₆, one H of both monomers takes part in the H:H contact interaction, producing a staggered configuration, which can thus be named 1:1s. Owing to the minimum number of interacting Hs, MM₁₆ is approximately half as stable as MM₁. As to the normal modes of MM₁₆, the lowest fundamental, mode #1, represents the (virtually free) rotation of the left methane monomer of Figure 1h around the C₁'–H₁' axis. Mode #1 is the fundamental which is predicted with a large relative error without RGC.

5.4. Methane Trimer, MMM. To the best of our knowledge, the methane trimer, MMM, has not been analyzed at high levels of electronic-structure theory. Some publications^{74–76} consider the “cyclic” (C_{3h}) structure as the global minimum of MMM, but the underlying computations do not go beyond the level of density functional theory. In the present study, a full geometry optimization and harmonic vibrational analysis have been conducted for this C_{3h} structure, called MMM_a, at the aug-cc-pVTZ MP2 level. This analysis resulted in a doubly degenerate imaginary mode around 6.8 i cm⁻¹. A

similar value, 8.6 i cm⁻¹, was obtained at the aug-cc-pVQZ MP2 level.

To detect a lower-order SP for MMM, small perturbations have been added to the atomic positions of MMM_a along the imaginary mode. Starting from this perturbed (initial) geometry, an aug-cc-pVTZ MP2 optimization was performed, leading to a minimum structure of C₂ point-group symmetry, named MMM_b. As MMM_b lies at a higher energy than MMM_a, MMM_b is only a local minimum at this level of theory. To find the true global minimum of MMM, higher-level electronic-structure computations are needed.

Assuming rigid monomers, constrained geometry optimizations have also been performed for MMM_a and MMM_b. The 12 intermolecular fundamentals obtained with different schemes are displayed in Table 6. The effect of the residual gradient is significant in the case of MMM; several noRGC(c) modes are not correct, not even qualitatively. The RGC₁ estimates show almost perfect agreement with their noRGC(u) counterparts: the largest unsigned deviation is 3 cm⁻¹ for the lowest-lying degenerate mode of MMM_a. The RGC₂ values are even more accurate, with the largest discrepancy less than 1 cm⁻¹.

6. CONCLUSIONS

Harmonic vibrational analyses at stationary points (SPs) obtained by geometry optimizations are important to (a) assess whether the SP determined is a minimum or a saddle point of arbitrary order and (b) provide a minimal under-

standing of the vibrational characteristics of the SP. Computing physically meaningful vibrational fundamentals of weakly bound oligomers becomes challenging if the SP is a constrained stationary point (cSP), obtained, for instance, within the rigid-monomer approximation and a constrained optimization. Since the gradient vector contains nonzero elements at a cSP, one faces the nonzero-force dilemma⁴⁶ during the derivation of normal modes.

In this study, an efficient code, called `oligoCGO`, is presented for the determination and the normal-mode vibrational analysis of cSPs. The `oligoCGO` code is able to (a) avoid occasional internal-coordinate singularities during the optimization steps, (b) ascertain the order of the cSP by evaluating the eigenvalues of the reduced-dimensional internal Hessian, and (c) cure the nonzero-force dilemma via two residual gradient correction (RGC) schemes.

RGC₁, which follows the recommendation of ref 46 and discards the remaining forces in an internal-coordinate system, is justified in the Appendix. RGC₂ modifies the cSP geometry in a single Newton step and the final Hessian is computed at this updated geometry. The RGC₂ scheme is more expensive than RGC₁, due to the fact that the Hessian needs to be evaluated twice. Nevertheless, the computational cost of the RGC₂ procedure can be reduced by replacing the Newton correction with a much cheaper quasi-Newton step.

To prove the utility of the RGC schemes implemented in `oligoCGO`, 10 stationary points, corresponding to the water–water, water–methane, and methane–methane dimers as well as the methane trimer, are examined. These examples confirm that the neglect of the remaining forces in Cartesian coordinates may yield even qualitatively incorrect vibrational fundamentals at cSPs. For instance, the cSP belonging to the global minimum of the water dimer has an incorrect imaginary mode when the constrained structure is that corresponding to rigid monomer units. In all the cases studied, RGC₁ and RGC₂ improve significantly the harmonic fundamentals of cSPs when referenced to the normal-mode wavenumbers of unconstrained SPs. The discrepancies of the RGC₁ and RGC₂ wavenumbers are typically less than 1–2 cm⁻¹ from the reference values.

Electronic-structure codes, at least those we are aware of, do not correct the normal-mode wavenumbers of cSPs for the residual gradients, because they simply work in Cartesian space. Therefore, the direct results of such quantum-chemical computations might be misleading. Developers of these codes may want to consider implementing the RGC₁ and RGC₂ schemes, helping users to obtain reasonable vibrational fundamentals at cSPs, without performing full geometry optimizations.

APPENDIX

To justify the approximation displayed in eq 7, one must return to the derivative relations presented in section 2.2. As a first step, $\partial^2 E / \partial X_j \partial X_k$ is rewritten via the chain rule,

$$\frac{\partial^2 E}{\partial X_j \partial X_k} = \sum_{l=1}^{\mathcal{Y}} \frac{\partial^2 E}{\partial q_l \partial X_k} \frac{\partial q_l}{\partial X_j} \quad (\text{A.1})$$

where ∂q_l and ∂X_k are not interchangeable as q_l and X_k are not independent of each other. By differentiating eq A.1 with respect to X_j , we obtain

$$\frac{\partial^3 E}{\partial X_i \partial X_j \partial X_k} = \sum_{l=1}^{\mathcal{Y}} \frac{\partial^3 E}{\partial X_i \partial q_l \partial X_k} \frac{\partial q_l}{\partial X_j} + \sum_{l=1}^{\mathcal{Y}} \frac{\partial^2 E}{\partial q_l \partial X_k} \frac{\partial^2 q_l}{\partial X_i \partial X_j} \quad (\text{A.2})$$

While the second sum of eq A.2 requires the knowledge of only second partial energy derivatives, the first sum depends on expensive third partial energy derivatives. Assuming the first sum to be much smaller than the second one, its neglect leads to

$$\begin{aligned} [[\mathbf{T}_{\text{Cart}}]]_{ijk} &= \frac{\partial^3 E}{\partial X_i \partial X_j \partial X_k} \approx \sum_{l=1}^{\mathcal{Y}} \frac{\partial^2 E}{\partial q_l \partial X_k} \frac{\partial^2 q_l}{\partial X_i \partial X_j} \\ &= \sum_{l=1}^{\mathcal{Y}} \sum_{p=1}^{\mathcal{C}} \frac{\partial^2 E}{\partial X_p \partial X_k} \frac{\partial X_p}{\partial q_l} \frac{\partial^2 q_l}{\partial X_i \partial X_j} \\ &= \sum_{p=1}^{\mathcal{C}} \sum_{l=1}^{\mathcal{Y}} [[\mathbf{A}^{(2)}]]_{jl} [[\mathbf{B}]]_{lp} [[\mathbf{H}_{\text{Cart}}]]_{pk} \\ &= [[\mathbf{A}^{(2)} \mathbf{B} \mathbf{H}_{\text{Cart}}]]_{ijk} \end{aligned} \quad (\text{A.3})$$

where $[[\]]$ denotes a specific entry of its argument tensor, and

$$\frac{\partial^2 E}{\partial q_l \partial X_k} = \sum_{p=1}^{\mathcal{C}} \frac{\partial^2 E}{\partial X_p \partial X_k} \frac{\partial X_p}{\partial q_l} \quad (\text{A.4})$$

is used to expand $\partial^2 E / \partial q_l \partial X_k$. Consequently, $\mathbf{T}_{\text{Cart}} \approx \mathbf{A}^{(2)} \mathbf{B} \mathbf{H}_{\text{Cart}}$ as stated in eq 7.

ASSOCIATED CONTENT

Supporting Information

The Supporting Information is available free of charge at <https://pubs.acs.org/doi/10.1021/acs.jctc.1c01148>.

Description of weakly bound oligomers, conversion of internal and Cartesian coordinate systems, discussion of LFR site choice, construction of connection lists, numerical calculation of transformation tensors, constrained geometry optimization, description of `oligoCGO` output files, and `oligoCGO` output files for WW1, WM1, WM7, MM1–MM4, MM16, MMM_a, and MMM_b (ZIP)

AUTHOR INFORMATION

Corresponding Author

Attila G. Császár – Institute of Chemistry, ELTE Eötvös Loránd University, Budapest 1117, Hungary; MTA-ELTE Complex Chemical Systems Research Group, Budapest 1117, Hungary; orcid.org/0000-0001-5640-191X; Email: attila.csaszar@ttk.elte.hu

Authors

Roland Tóbiás – Institute of Chemistry, ELTE Eötvös Loránd University, Budapest 1117, Hungary; MTA-ELTE Complex Chemical Systems Research Group, Budapest 1117, Hungary
Péter Arendás – MTA-ELTE Complex Chemical Systems Research Group, Budapest 1117, Hungary; Budapest Business School, Budapest 1149, Hungary; Institute of Chemistry, ELTE Eötvös Loránd University, Budapest 1117, Hungary

Complete contact information is available at: <https://pubs.acs.org/10.1021/acs.jctc.1c01148>

Notes

The authors declare no competing financial interest.

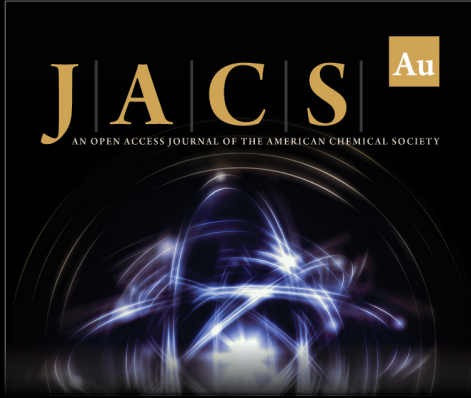
ACKNOWLEDGMENTS

The work performed was supported by Grant VEKOP-2.3.2-16-2017-000 and by NKFIH (Grant Number: K138233). Dr. László Gyevi-Nagy is thanked for fruitful discussions. R.T. is grateful to Mrs. Marietta Tóbiásné Zseni for her assistance in the design of Figure 1.

REFERENCES

- (1) Pulay, P. In *Modern Theoretical Chemistry*; Schaefer, H. F., III, Ed.; Plenum: New York, 1977; Vol. 4, pp 153–185.
- (2) Murrell, J. N.; Carter, S.; Farantos, S. C.; Huxley, P.; Varandas, A. J. C. *Molecular potential energy functions*; Wiley: New York, 1984.
- (3) Mezey, P. G. *Potential energy hypersurfaces*; Elsevier: New York, 1987.
- (4) Császár, A. G.; Allen, W. D.; Yamaguchi, Y.; Schaefer, H. F., III. In *Computational molecular spectroscopy*; Jensen, P., Bunker, P. R., Eds.; Wiley: Chichester, 2000; pp 15–68.
- (5) Marx, D.; Hutter, J. *Ab initio Molecular Dynamics: Basic Theory and Advanced Methods*; Cambridge University Press: Cambridge, 2009.
- (6) Császár, A. G.; Fábri, C.; Szidarovszky, T.; Mátyus, E.; Furtenbacher, T.; Czako, G. The fourth age of quantum chemistry: molecules in motion. *Phys. Chem. Chem. Phys.* **2012**, *14*, 1085–1106.
- (7) Metz, M. P.; Piszczatowski, K.; Szalewicz, K. Automatic generation of intermolecular potential energy surfaces. *J. Chem. Theory Comput.* **2016**, *12*, 5895–5919.
- (8) Metz, M. P.; Szalewicz, K. Automatic generation of flexible-monomer intermolecular potential energy surfaces. *J. Chem. Theory Comput.* **2020**, *16*, 2317–2339.
- (9) Born, M.; Oppenheimer, J. R. Zur quantentheorie der molekeln. *Ann. Phys. (Berlin)* **1927**, *389*, 457–484.
- (10) Born, M.; Huang, K. *Dynamical theory of crystal lattices*; Clarendon Press: Oxford, 1954.
- (11) Császár, A. G.; Tarczay, G.; Leininger, M. L.; Polyansky, O. L.; Tenynson, J.; Allen, W. D. In *Spectroscopy from Space*; Demaison, J., Sarka, K., Cohen, E. A., Eds.; Kluwer: Dordrecht, 2001; pp 317–339.
- (12) Volkenstein, M. V.; El'yashevich, M. A.; Stepanov, B. I. *Kolebanija Molekul*; Gostechizdat: Moscow, 1949.
- (13) Wilson, E. B., Jr.; Decius, J. C.; Cross, P. C. *Molecular vibrations: the theory of infrared and Raman vibrational spectra*; McGraw Hill: New York, 1955.
- (14) Schlegel, H. B. Optimization of equilibrium geometries and transition structures. *J. Comput. Chem.* **1982**, *3*, 214–218.
- (15) Simons, J.; Jorgensen, P.; Taylor, H.; Ozment, J. Walking on potential energy surfaces. *J. Phys. Chem.* **1983**, *87*, 2745–2753.
- (16) Császár, P.; Pulay, P. Geometry optimization by direct inversion in the iterative subspace. *J. Mol. Struct. (Theochem)* **1984**, *114*, 31–34.
- (17) Pulay, P.; Fogarasi, G. Geometry optimization in redundant internal coordinates. *J. Chem. Phys.* **1992**, *96*, 2856–2860.
- (18) Peng, C.; Ayala, P. Y.; Schlegel, H. B.; Frisch, M. J. Using redundant internal coordinates to optimize equilibrium geometries and transition states. *J. Comput. Chem.* **1996**, *17*, 49–56.
- (19) Paizs, B.; Baker, J.; Suhai, S.; Pulay, P. Geometry optimization of large biomolecules in redundant internal coordinates. *J. Chem. Phys.* **2000**, *113*, 6566–6572.
- (20) Farkas, O.; Schlegel, H. B. Methods for optimizing large molecules. Part III. An improved algorithm for geometry optimization using direct inversion in the iterative subspace (GDIIS). *Phys. Chem. Chem. Phys.* **2002**, *4*, 11–15.
- (21) Schlegel, H. B. Geometry optimization. *WIREs Comput. Mol. Sci.* **2011**, *1*, 790–809.
- (22) Hobza, P.; Müller-Dethlefs, K. *Non-Covalent Interactions: Theory and Experiment*; Royal Society of Chemistry: London, 2010.
- (23) Pauling, L. *The nature of the chemical bond*; Cornwall University Press: New York, 1939.
- (24) Richardson, T.; de Gala, S.; Crabtree, R. H.; Siegbahn, P. E. M. Unconventional hydrogen bonds: Intermolecular B–H–H–N interactions. *J. Am. Chem. Soc.* **1995**, *117*, 12875–12876.
- (25) Alkorta, I.; Elguero, J.; Foces-Foces, C. Dihydrogen bonds (A–H–H–B). *Chem. Commun.* **1996**, 1633–1634.
- (26) Echeverría, J.; Aullón, G.; Danovich, D.; Shaik, S.; Alvarez, S. Dihydrogen contacts in alkanes are subtle but not faint. *Nat. Chem.* **2011**, *3*, 323–330.
- (27) Nishio, M. CH/ π hydrogen bonds in crystals. *CrystEngComm* **2004**, *6*, 130–158.
- (28) Janiak, C. A critical account on π – π stacking in metal complexes with aromatic nitrogen-containing ligands. *Dalton Trans.* **2000**, 3885–3896.
- (29) Metrangolo, P.; Meyer, F.; Pilati, T.; Resnati, G.; Terraneo, G. Halogen bonding in supramolecular chemistry. *Angew. Chem., Int. Ed.* **2008**, *47*, 6114–6127.
- (30) Metrangolo, P.; Resnati, G. *Halogen Bonding: Fundamentals and Applications*; Springer: Berlin, 2008.
- (31) Aakeroy, C. B.; Bryce, D. L.; Desiraju, G. R.; Frontera, A.; Legon, A. C.; Nicotra, F.; Rissanen, K.; Scheiner, S.; Terraneo, G.; Metrangolo, P.; Resnati, G. Definition of the chalcogen bond (IUPAC Recommendations 2019). *Pure Appl. Chem.* **2019**, *91*, 1889–1892.
- (32) Marcus, Y.; Hefter, G. Ion pairing. *Chem. Rev.* **2006**, *106*, 4585–4621.
- (33) Brookhart, M.; Green, M. L. H.; Parkin, G. Agostic interactions in transition metal compounds. *Proc. Natl. Acad. Sci. U.S.A.* **2007**, *104*, 6908–6914.
- (34) Dougherty, D. A. Cation- π interactions in chemistry and biology: a new view of benzene, Phe, Tyr, and Trp. *Science* **1996**, *271*, 163–168.
- (35) Ma, J. C.; Dougherty, D. A. The cation- π interaction. *Chem. Rev.* **1997**, *97*, 1303–1324.
- (36) Papp, D.; Rovó, P.; Jákl, I.; Császár, A. G.; Perczel, A. Four faces of the interaction between ions and aromatic rings. *J. Comput. Chem.* **2017**, *38*, 1762–1773.
- (37) Kaplan, I. G. *Intermolecular Interactions*; Wiley: Chichester, 2006.
- (38) Baker, J. An algorithm for the location of transition states. *J. Comput. Chem.* **1986**, *7*, 385–395.
- (39) Lu, D.-H.; Zhao, M.; Truhlar, D. G. Projection operator method for geometry optimization with constraints. *J. Comput. Chem.* **1991**, *12*, 376–384.
- (40) Baker, J. Geometry optimization in Cartesian coordinates: Constrained optimization. *J. Comput. Chem.* **1992**, *13*, 240–253.
- (41) Baker, J. Techniques for geometry optimization: A comparison of Cartesian and natural internal coordinates. *J. Comput. Chem.* **1993**, *14*, 1085–1100.
- (42) Anglada, J. M.; Bofill, J. M. A reduced-restricted-quasi-Newton-Raphson method for locating and optimizing energy crossing points between two potential energy surfaces. *J. Comput. Chem.* **1997**, *18*, 992–1003.
- (43) De Vico, L.; Olivucci, M.; Lindh, R. New general tools for constrained geometry optimizations. *J. Chem. Theory Comput.* **2005**, *1*, 1029–1037.
- (44) Budzelaar, P. H. M. Geometry optimization using generalized, chemically meaningful constraints. *J. Comput. Chem.* **2007**, *28*, 2226–2236.
- (45) Stenrup, M.; Lindh, R.; Galván, I. F. Constrained numerical gradients and composite gradients: Practical tools for geometry optimization and potential energy surface navigation. *J. Comput. Chem.* **2015**, *36*, 1698–1708.
- (46) Allen, W. D.; Császár, A. G. On the ab initio determination of higher-order force constants at nonstationary reference geometries. *J. Chem. Phys.* **1993**, *98*, 2983–3015.
- (47) Császár, A. G. Anharmonic molecular force fields. *WIREs Comput. Mol. Sci.* **2012**, *2*, 273–289.

- (48) Papoušek, D.; Aliev, M. R. *Molecular vibrational-rotational spectra*; Elsevier: New York, 1982.
- (49) Schwendeman, R. H. Application of the Hellmann-Feynman and virial theorems to the theoretical calculation of molecular potential constants. *J. Chem. Phys.* **1966**, *44*, 556–561.
- (50) Schwendeman, R. H. Comparison of experimentally derived and theoretically calculated derivatives of the energy, kinetic energy, and potential energy for CO. *J. Chem. Phys.* **1966**, *44*, 2115–2119.
- (51) Pulay, P.; Fogarasi, G.; Pang, F.; Boggs, J. E. Systematic *ab initio* gradient calculation of molecular geometries, force constants, and dipole moment derivatives. *J. Am. Chem. Soc.* **1979**, *101*, 2550–2560.
- (52) Baker, J.; Pulay, P. Efficient geometry optimization of molecular clusters. *J. Comput. Chem.* **2000**, *21*, 69–76.
- (53) Bakken, V.; Helgaker, T. The efficient optimization of molecular geometries using redundant internal coordinates. *J. Chem. Phys.* **2002**, *117*, 9160–9174.
- (54) Zhang, J.; Dolg, M. Global optimization of clusters of rigid molecules using the artificial bee colony algorithm. *Phys. Chem. Chem. Phys.* **2016**, *18*, 3003–3010.
- (55) Allen, W. D.; Császár, A. G.; Szalay, V.; Mills, I. M. General derivative relations for anharmonic force fields. *Mol. Phys.* **1996**, *89*, 1213–1221.
- (56) Simons, J.; Jørgensen, P.; Taylor, H.; Ozment, J. Walking on potential energy surfaces. *J. Phys. Chem.* **1983**, *87*, 2745–2753.
- (57) Peng, C.; Schlegel, B. H. Combining synchronous transit and quasi-newton methods to find transition states. *Isr. J. Chem.* **1993**, *33*, 449–454.
- (58) Banerjee, A.; Adams, N.; Simons, J.; Shepard, R. Search for stationary points on surfaces. *J. Phys. Chem.* **1985**, *89*, 52–57.
- (59) Allen, W. D.; East, A. L. L.; Császár, A. G. In *Structures and Conformations of Nonrigid Molecules*; Laane, J., Dakkouri, M., van der Veken, B., Oberhammer, H., Eds.; Kluwer: Dordrecht, 1993; pp 343–373.
- (60) Vibrational analysis in Gaussian, last accessed on January 19, 2022.
- (61) Frisch, M. J. et al. *Gaussian16*, rev. B.01; Gaussian Inc.: Wallingford, CT, 2016.
- (62) Gyevi-Nagy, L.; Tasi, G. SYVA: a program to analyze symmetry of molecules based on vector algebra. *Comput. Phys. Commun.* **2017**, *215*, 156–164.
- (63) Tasi, G.; Gyevi-Nagy, L.; Tóbiás, R.; Tasi, T. S. Vector algebra and molecular symmetry: a tribute to Professor Josiah Willard Gibbs. *J. Math. Chem.* **2013**, *51*, 2187–2195.
- (64) Metz, M. P.; Szalewicz, K.; Sarka, J.; Tóbiás, R.; Császár, A. G.; Mátyus, E. Molecular dimers of methane clathrates: *ab initio* potential energy surfaces and variational vibrational states. *Phys. Chem. Chem. Phys.* **2019**, *21*, 13504–13525.
- (65) Møller, C.; Plesset, M. S. Note on an approximation treatment for many-electron systems. *Phys. Rev.* **1934**, *46*, 618–622.
- (66) Dunning, T. H., Jr. Gaussian basis sets for use in correlated molecular calculations. I. The atoms boron through neon and hydrogen. *J. Chem. Phys.* **1989**, *90*, 1007–1023.
- (67) Tóbiás, R.; Császár, A. G.; Gyevi-Nagy, L.; Tasi, G. Definitive thermochemistry and kinetics of the interconversions among conformers of *n*-butane and *n*-pentane. *J. Comput. Chem.* **2018**, *39*, 424–437.
- (68) Boys, S. F.; Bernardi, F. The calculation of small molecular interactions by the differences of separate total energies. Some procedures with reduced errors. *Mol. Phys.* **1970**, *19*, 553–566.
- (69) Simon, S.; Duran, M.; Dannenberg, J. J. How does basis set superposition error change the potential surfaces for hydrogen bonded dimers? *J. Chem. Phys.* **1996**, *105*, 11024–11031.
- (70) Akin-Ojo, O.; Szalewicz, K. Potential energy surface and second virial coefficient of methane-water from *ab initio* calculations. *J. Chem. Phys.* **2005**, *123*, 134311.
- (71) Copeland, K. L.; Tschumper, G. S. Hydrocarbon/water interactions: Encouraging energetics and structures from DFT but disconcerting discrepancies for Hessian indices. *J. Chem. Theory Comput.* **2012**, *8*, 1646–1656.
- (72) Qu, C.; Conte, R.; Houston, P. L.; Bowman, J. M. “Plug and play” full-dimensional *ab initio* potential energy and dipole moment surfaces and anharmonic vibrational analysis for CH₄–H₂O. *Phys. Chem. Chem. Phys.* **2015**, *17*, 8172–8181.
- (73) Rivera-Arrieta, H. I.; Turney, J. M.; Schaefer, H. F., III Structural distortions accompanying noncovalent interactions: Methane–water, the simplest C–H hydrogen bond. *J. Chem. Theory Comput.* **2017**, *13*, 1478–1485.
- (74) Szczęśniak, M.; Chalaśiński, G.; Cybulski, S.; Scheiner, S. Intermolecular potential of the methane dimer and trimer. *J. Chem. Phys.* **1990**, *93*, 4243–4253.
- (75) Takeuchi, H. The structural investigation on small methane clusters described by two different potentials. *Comput. Theor. Chem.* **2012**, *986*, 48–56.
- (76) Torres, E.; Di Labio, G. A. Density-functional theory with dispersion-correcting potentials for methane: Bridging the efficiency and accuracy gap between high-level wave function and classical molecular mechanics methods. *J. Chem. Theory Comput.* **2013**, *9*, 3342–3349.



JACS Au
AN OPEN ACCESS JOURNAL OF THE AMERICAN CHEMICAL SOCIETY

Editor-in-Chief
Prof. Christopher W. Jones
Georgia Institute of Technology, USA

Open for Submissions

pubs.acs.org/jacsau
ACS Publications
Most Trusted. Most Cited. Most Read.